Dense shelf water formation process in the Sea of Okhotsk based on an ice-ocean coupled model

Ayumi Fujisaki,[1,2] Humio Mitsudera,[3] and Hajime Yamaguchi[1]

[1] Formation process of the dense shelf water (DSW) in the Sea of Okhotsk was investigated with an ice-ocean coupled model. The hindcast through 1998–2000 modeled the anomalous ice productions being controlled by air temperature and mean ice speed over the coastal area. Ice production was larger by 30% in 1998–1999, while less developed ice cover in 1999–2000 allowed larger heat loss from the ocean. The compensating heat loss sustained the similar production of the DSW for $>26.75\sigma_\theta$ in 1998–1999. However, ice production thickened up the density constitution of the DSW, which was significantly denser in 1998–1999. An experiment without brine rejection suggested such modification of the density constitution plays a rather more important role in brine rejection for the DSW property than an increase of the volumetric production. The signal of brine rejection reached the $27\sigma_\theta$ layer farther south in the Kuril Basin. The model also showed that when winter outflow of the DSW from the continental shelf was neglected, as is the case in observational estimations, the annual production was underestimated by 20% compared with actual productions in 1998–2000. Ice production was increased as the air-ice drag coefficient C_{Dai} increased and as the ice-water drag coefficient C_{Diw} decreased because of the intensified polynya activity. In contrast, the density constitution of the DSW was lightened with the increased C_{Dai}, as a linear balance of dominantly intensified advection and slight increase of ice production. Consequently, the DSW property seemed insensitive to C_{Dai} and C_{Diw} compared with the anomalous air conditions year by year.

Citation: Fujisaki, A., H. Mitsudera, and H. Yamaguchi (2011), Dense shelf water formation process in the Sea of Okhotsk based on an ice-ocean coupled model, *J. Geophys. Res.*, *116*, C03005, doi:10.1029/2009JC006007.

1. Introduction

[2] The dense shelf water (DSW) in the Sea of Okhotsk has significant roles in a meridional overturning in the northwest Pacific. The DSW is produced in the northern continental shelf region of the Sea of Okhotsk where sea ice is actively produced, sinks to a depth of about 200–500 m, and is transported southward along the Sakhalin coast [*Fukamachi et al.*, 2004]. The water mass transported to the southern region of the Sea of Okhotsk goes through the strong tidal mixing along the Kuril Islands [*Nakamura et al.*, 2006; *Nakamura and Awaji*, 2004], and ultimately, this water becomes a ventilation source of the North Pacific Intermediate Water [*Shcherbina et al.*, 2003, 2004a, 2004b]. Thus,

the DSW significantly influences the intermediate circulation in the North Pacific [*Nakamura et al.*, 2006; *Nakanowatari et al.*, 2007]. Besides, the DSW is likely to play important roles in biochemical processes. Atmospheric gases (e.g., CO_2, O_2, and CFC) and nutrient materials (e.g., iron) are dissolved up and transported from the continental shelf to the deeper layer [*Yamamoto-Kawai et al.*, 2004; *Nishioka et al.*, 2007]. Since such tracer circulation can involve a broad range of density layers, it is important to know the contribution of brine rejection to the DSW penetration.

[3] There are several indirect estimates of the DSW formation [*Gladyshev et al.*, 2000, 2003; *Itoh et al.*, 2003]. *Itoh et al.* [2003] estimated the annual production rate of 0.67 Sv based on historical hydrographic data. *Shcherbina et al.* [2003, 2004a, 2004b] measured the brine rejection process in the northwest polynya. One earlier numerical model approach by *Matsuda et al.* [2009] proposed the meridional overturning in the Sea of Okhotsk, in which the transported saline water is returned to the northern shelf region by the strong tidal mixing along the Kuril Islands and wind-driven circulation, resulting in the promotion of DSW production. Their model is forced by the climatological atmosphere, and, therefore, it is difficult to validate the results based on the observations.

[1] Graduate School of Frontier Science, University of Tokyo, Tokyo, Japan.
[2] Now at Cooperative Institute for Limnology and Ecosystems Research, School of Natural Resources and Environment, University of Michigan, Great Lakes Environmental Research Laboratory, NOAA, Ann Arbor, Michigan, USA.
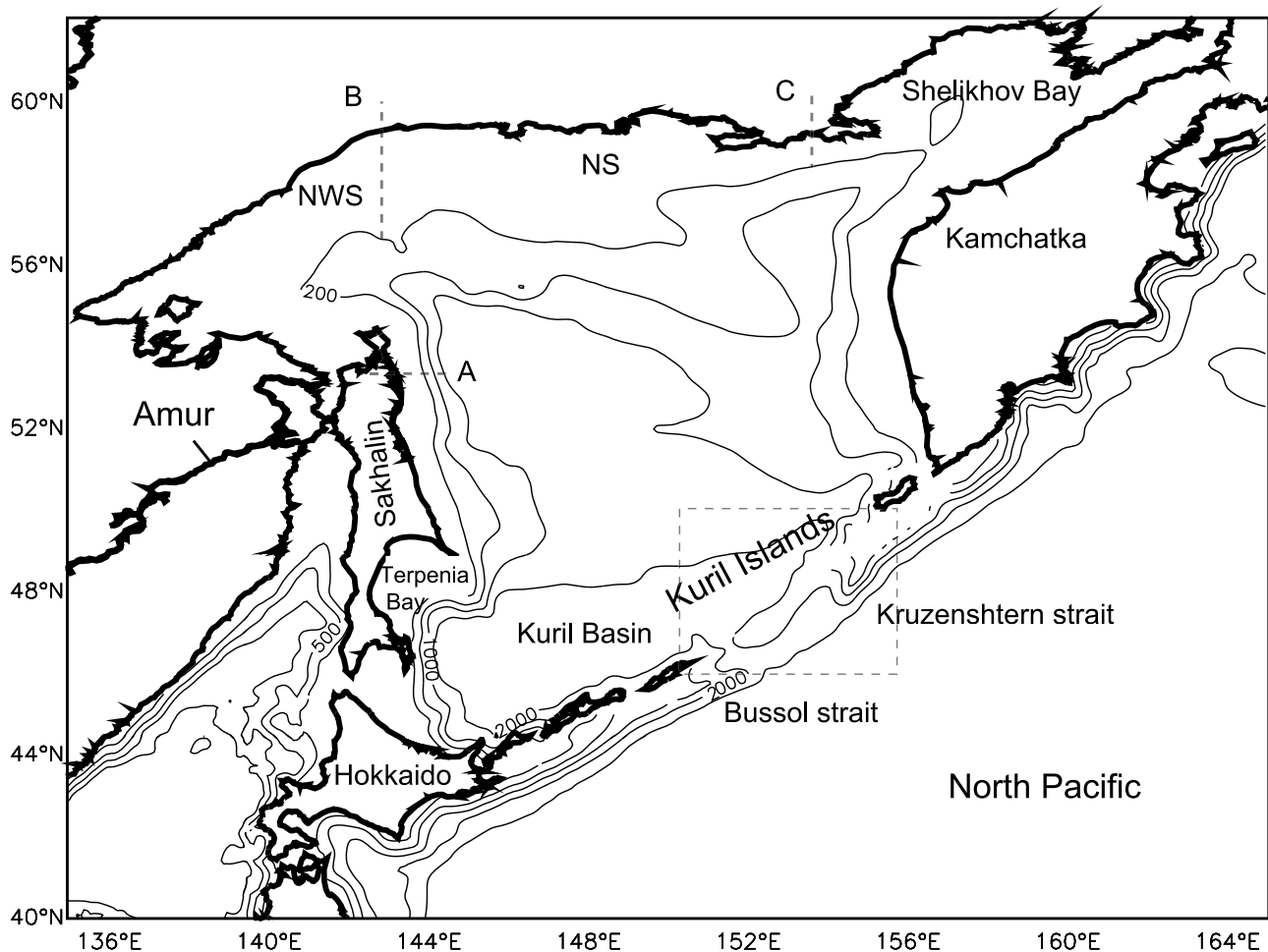[3] Institute of Low Temperature Science, Hokkaido University, Sapporo, Japan.

Figure 1. Topography of the Sea of Okhotsk in the model. Contours denote the depth (m). Region surrounded by a dashed line is enlarged in Figure 2. Lines are A (53°N), B (143°E), and C (154°E).

[4] Our study aims to reproduce a DSW formation process using the actual atmospheric forcing during 1998–2000, which includes the observation period of *Shcherbina et al.* [2003, 2004a, 2004b]. In the winter of 1999–2000, the atmospheric condition was milder than that of 1998–1999, and the anomaly of air temperature over the northern part of the Sea of Okhotsk is strongly positive by roughly 3° from the 10 year mean field (Figure 6, discussed in section 3). The model forced by this anomalous air temperature year by year would predict anomalous ice production, which is expected to be larger in 1998–1999 and smaller in 1999–2000, and formed DSW could represent the anomalous ice production. We will discuss the interannual variation of ice production and the impacts on the DSW property based on the model results for the two seasons.

[5] The impact of brine rejection on the DSW formation is another point of interest. Very dense brine is expected to contribute to thickening up the DSW and modify the density constitution of the DSW. We will carry out a simple experiment in which brine rejection is artificially turned off to evaluate how much brine rejection could affect the density constitution and the volumetric production of the DSW.

[6] One issue to be validated is sensitivity of the model to the air-ice drag coefficient C_{Dai} and the ice-water drag coefficient C_{Diw} because their values are quite uncertain but can have a significant impact on ice production. Wind stress is a significant factor for polynya activity, and the drag coefficients that determine the wind stress need to be set properly to correctly predict ice production and DSW production.

[7] In addition, C_{Dai} may affect the density constitution of the DSW by determining the alongshore flow speed as a balance of advection and feeding speed of brine [*Kawaguchi and Mitsudera*, 2009]. C_{Dai} controls the volume transport of the East Sakhalin Current (ESC) [*Fujisaki et al.*, 2010], and, therefore, the sensitivity of C_{Dai} on the density constitution of the DSW should be evaluated.

[8] Generally the uncertainty in C_{Dai} and C_{Diw} arises due to the various topography of sea ice. Intensive ridging and rafting make the ice surface and base rough (larger C_{Dai} and C_{Diw}), while pure congelation makes them smooth and flat (small C_{Dai} and C_{Diw}). Typical values for C_{Dai} and C_{Diw} depend on the regions. Although some numerical models treat C_{Dai} as a function of ice thickness, such a function is based on a simple assumption that thick ice has a large C_{Dai} because they have gone through more rifting and rafting.

Table 1. Settings of Model Parameters

Variable	Description	Value
dt_{ext}	time step in external mode	8 s
dt_{int}	time step in internal mode and ice thermodynamic model	480 s
dt_{ice}	time step in ice dynamic model	60 s
K_b	background value for the vertical eddy viscosity and diffusivity	5.0×10^{-5} m^2 s^{-1}
$P*$	compressive strength	50 kPa
C	compaction hardening	20
$P*_{col}$	parameter which determines the strength of floe collision	10^{12} Pa s^2
C_{col}	parameter which determine the switching ratio to floe collision mode	20
d	constant in floe collision rheology	0.01
E_0	constant for elastic coefficient in ice dynamic model	0.25
n_{sub}	number of substeps in calculating the ice internal stress	10
C_{Dai}	air-ice drag coefficient (changed in the sensitivity studies)	3.0×10^{-3} (basic)
C_{Diw}	ice-water drag coefficient (changed in the sensitivity studies)	9.0×10^{-3} (basic)
C_{hs}	turbulent sensible heat transfer coefficient	1.75×10^{-3}
C_{hl}	turbulent latent heat transfer coefficient	1.75×10^{-3}
C_{hio}	turbulent ice-ocean heat transfer coefficient	5.0×10^{-3}
α_w	albedo of open water surface	0.1
α_i	albedo of sea ice surface	0.7
c_{pa}	specific heat of the air	1004.0 J kg^{-1} K^{-1}
c_{pw}	specific heat of seawater	4000.0 J kg^{-1} K^{-1}
ρ_a	density of the air	1.247 kg m^{-3}
ρ_i	density of sea ice	910.0 kg m^{-3}
s_i	salinity of sea ice	0.0
L_e	evaporative latent heat of seawater	2.5×10^6 J kg^{-1}
L_i	melting latent heat of sea ice	3.3×10^5 J kg^{-1}
L_s	sublimation latent heat of sea ice	2.8×10^6 J kg^{-1}
ε_w	longwave emissivity of seawater	0.97
ε_i	longwave emissivity of sea ice	0.97

Such a function is still empirical and does not certify a proper value without sufficient observations in a region of interest.

[9] In the Sea of Okhotsk, a few measurements by *Shirasawa* [1981] and *Fujisaki et al.* [2009] show a wide range of C_{Dai} 1.9–5.4 $\times 10^{-3}$. Hence a sensitivity study is necessary to evaluate the uncertainty of a model caused by C_{Dai}.

[10] In terms of C_{Diw}, the number of observation is much smaller because of the difficulty of measurements underneath ice and there is almost no observation in the Sea of Okhotsk. However, we can cite the observational fact that the ratio of C_{Dai} to C_{Diw} in geostrophic reference ranges from 0.2 to 0.8 [*Leppäranta*, 2005]. We focus on the impact of the C_{Dai} and C_{Diw} values on ice production and DSW production.

[11] In section 2, the model used in this study and the detailed settings in the sensitivity study are described. In section 3, the model results are validated based on sea ice distribution and the observations by *Shcherbina et al.* [2003, 2004a, 2004b]. An interannual variability through 1998–2000 is also discussed in terms of ice production and DSW
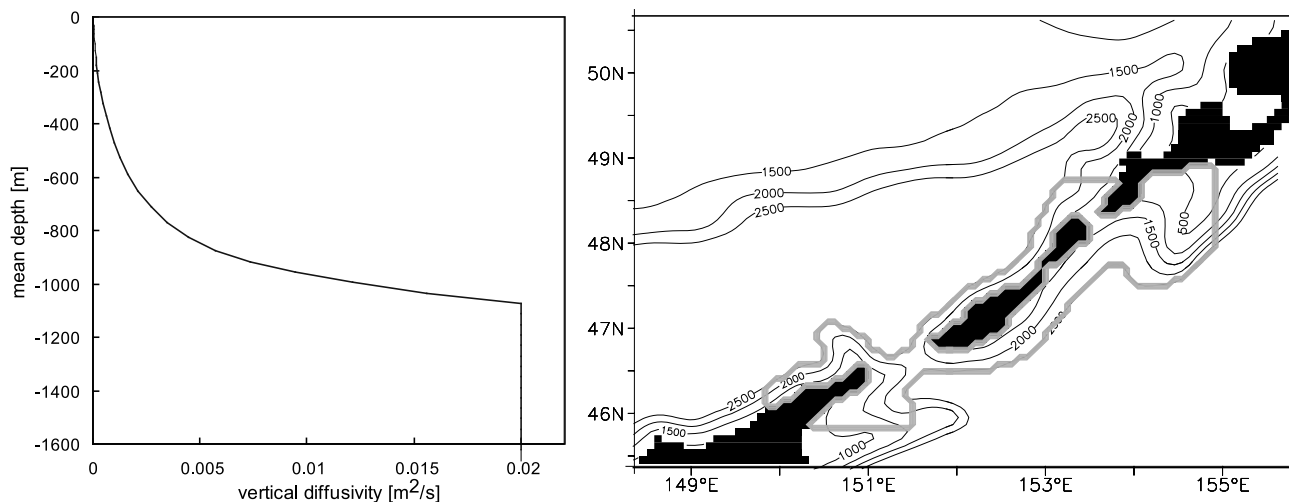

Figure 2. (right) Topography around the Bussol Strait and the Kruzenshtern Strait. (left) Lower bound of the vertical eddy viscosity and diffusivity in the region surrounded by a gray line.

Table 2. Numerical Experiments

Experiment	Title of Experiment	Note
1	basic	$C_{Dai} \times 10^3 = 3.0$, $C_{Diw} \times 10^3 = 9.0$
2	no brine rejection	no salt flux due to freezing/melting
3	sensitivity study of air-ice drag coefficient C_{Dai}	$C_{Dai} \times 10^3 = 2.0, 4.0, 5.0$, $C_{Diw} \times 10^3 = 9.0$
4	sensitivity study of ice-water drag coefficient C_{Diw}	$C_{Dai} \times 10^3 = 3.0$, $C_{Diw} \times 10^3 = 3.0, 6.0$

formation. In section 4, the sensitivities of ice production, volumetric production of the DSW, and its density constitution to the drag coefficients and brine rejection are discussed based on the model results. We summarize the model study in section 5.

2. Model

2.1. Ice-Ocean Coupled Model

[12] A high-resolution ice-ocean coupled model in a regional domain is used to study formation of the DSW in the Sea of Okhotsk. The model configuration is almost the same as that of *Fujisaki et al.* [2010]. The computational domain is shown in Figure 1. Resolution has 1/12° grids horizontally and 45 layers vertically. The topography is based on GETECH DTM5. The ocean part is based on the Princeton Ocean Model, which employs the primitive equations and a generalized sigma coordinate (see *Uchimoto et al.* [2007] for details). The ice dynamic model employs the elastic-viscous-plastic rheology [*Hunke and Duckowicz*, 1997] and also takes into account the ice collision [*Fujisaki*

et al., 2010; *Sagawa*, 2007]. A detailed description of the ice collision rheology and its impacts in the Sea of Okhotsk are given by *Fujisaki et al.* [2010]. The ice thermodynamic part is based on the zero-layer thermodynamic model [*Semtner*, 1976]. The settings of the model parameters are listed in Table 1.

[13] The lateral boundary conditions are given by the five daily model results of the Japan Coastal Ocean Predictability Experiment (JCOPE), so that the model can take into account the East Kamchatka Current, Tsushima Warm Current, and Soya Warm Current. Since our model does not include a tide model, the strong tidal mixing along the Kuril Islands cannot be solved explicitly. In order to include the strong tidal mixing, a lower limit of the vertical diffusivity and the vertical viscosity along the Kuril Islands is specified (Figure 2).

[14] The atmospheric forcings are given every 12 h by the objective analysis of the Regional Spectral Model, compiled by the Japan Meteorological Agency through 1998–2000. Note that the meridional and zonal components of the mean wind velocities are multiplied by 1.25 because we found that
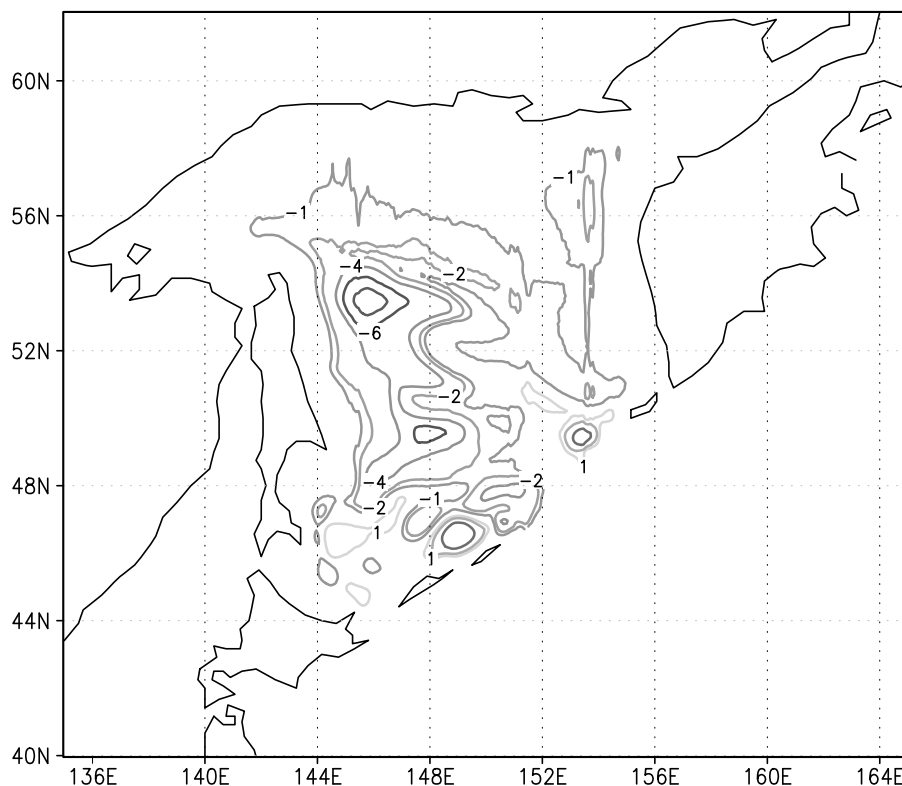

Figure 3. Stream function of the basic experiment, averaged from October 1998 to September 2000. Contour denotes a volume transport (Sv). The interval is 2 Sv and ±1 Sv are also shown.
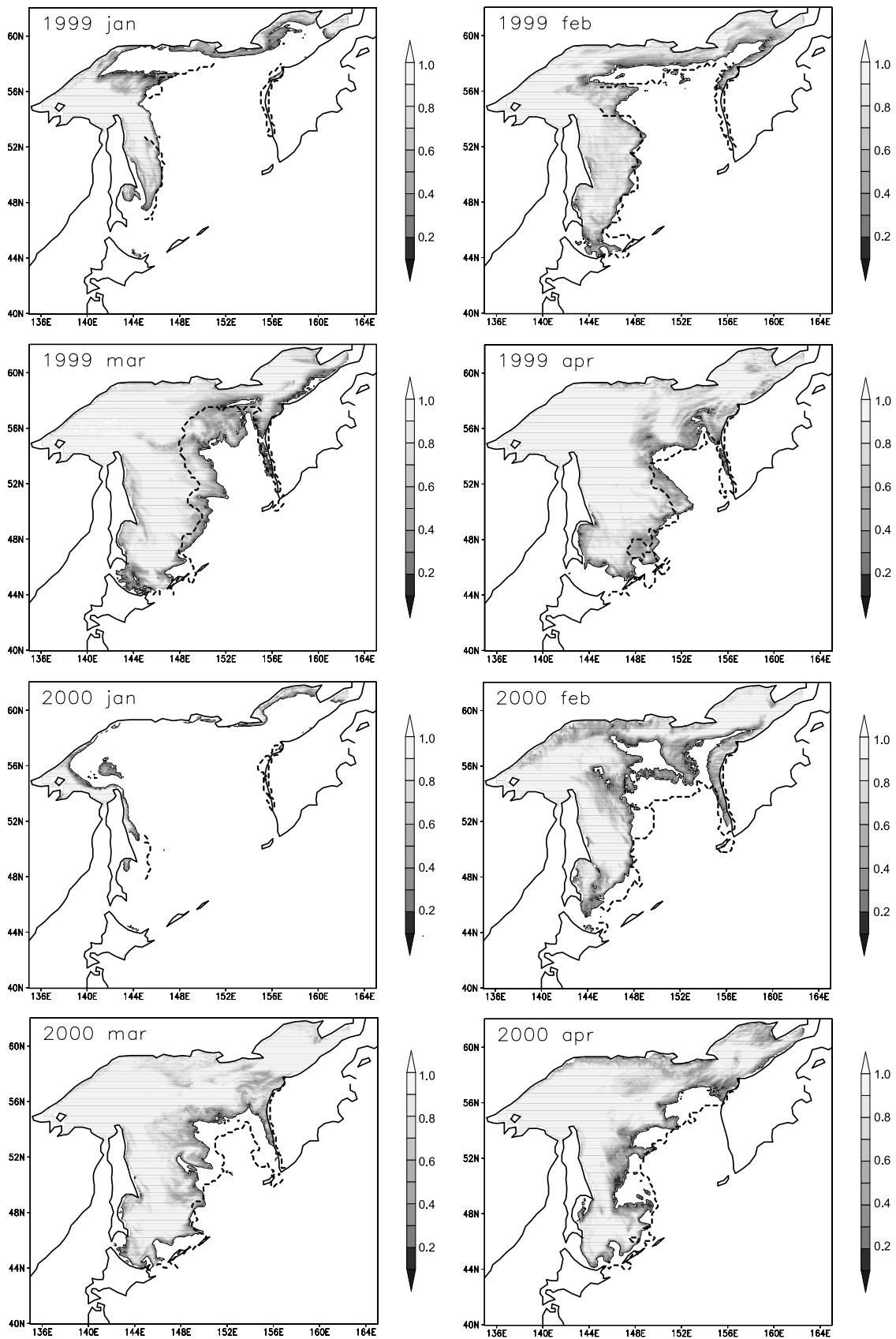
Figure 4. Ice concentrations in the basic experiment averaged over 1–5 of each month. This is the same as Figure 4 of *Fujisaki et al.* [2010]. Lines indicate ice edges (ice concentration of 0.1). Dashed lines are sea ice analysis compiled by the Japan Meteorological Agency. Solid lines are model result of the basic experiment.
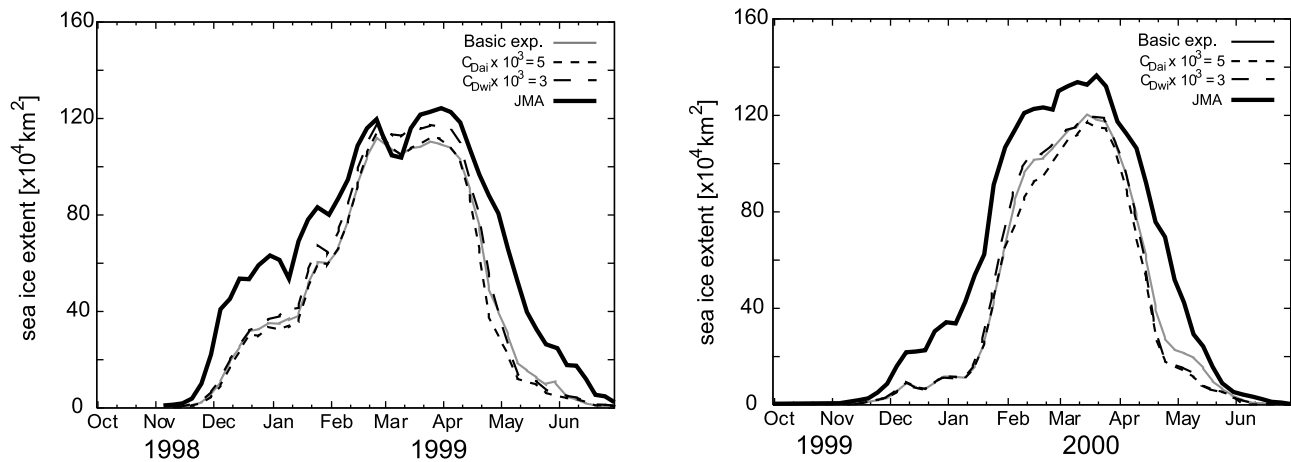
Figure 5. Time series of sea ice extent in the Sea of Okhotsk, which ha s a total area of ice concentration higher than 0.1. Thick solid line is from the sea ice analysis of the Japan Meteorological Agency. This is the same as Figure 5 of *Fujisaki et al.* [2010]. Thin solid and dashed lines are from the sensitivity experiments of the air-ice drag coefficient C_{Dai} and the ice-water drag coefficient C_{Diw}.

the wind velocity over the Sea of Okhotsk from 1998 to 2000 is weaker than that of the National Centers for Environmental Prediction (NCEP)-Department of Energy (DOE) Atmospheric Model Intercomparison Project (AMIP)-II reanalysis with regression coefficients of 1.22 for the meridional component and 1.26 for the zonal component. The wind stress over sea surface is calculated by the formulation of *Large and Pond* [1981], and those over and under sea ice are calculated by similar equations

$$\vec{\tau}_{ai} = \rho_a C_{Dai} |\vec{U}_a| \vec{U}_a \tag{1}$$

$$\vec{\tau}_{iw} = \rho_w C_{Dwi} |\vec{U}_i - \vec{U}_w| (\vec{U}_i - \vec{U}_w). \tag{2}$$

Here, ρ_a and ρ_w are the density of air and seawater, respectively. U_a denotes the mean wind speed at 10 m height. U_i is the ice drift velocity, and U_w is the sea surface velocity. C_{Dai} and C_{Diw} are the air-ice drag coefficient and ice-water drag coefficient, respectively.

[15] The shortwave radiation, longwave radiation, sensible heat flux, and latent heat flux are calculated for ice surface and sea surface. The sea surface salinity is restored to the analysis of monthly climatology (K. I. Ohshima, unpublished data, 2008) with a relaxation scale of 30 days for the top level of the model, which is 10 m thick

$$Q_s = \frac{dQ_s}{ds} (s_1 - s_a), \tag{3}$$

where Q_s is a sea surface salt flux by restoring. Here, s_1 and s_a are salinity in the top layer and analysis, respectively. Here, dQ_s/ds = 10 m/30 days is a relaxation factor. The factor is also used in shelf regions whose top layer thickness is less than 10 m, where, therefore, relaxation may work more strongly. Equation (2) is weighted by $1 - A$ over a calculation cell where A is ice concentration. This suppressing of restoration under ice is done in order not to relax a salt plume effect by brine rejection.

[16] The time integration starts from the steady state with a climatological temperature and salinity field [*Levitus et al.*, 1994]. The model was spun up to 15 years without the ice model, and then for an additional 8 years with the ice model. The atmospheric forcing during 1998–2000 is repeated during the numerical integration, and the analyses are done for the last two winters.

2.2. Numerical Experiments

[17] One interest in this study is to evaluate the impacts of brine rejection on the density constitution of the DSW. We carry out an experiment in which sea ice keeps the same salinity as seawater to see the modification of the DSW caused by brine rejection. In this experiment, there is no salt flux by ice formation, nor by ice melting. The experiment without brine rejection was carried out for the last 3 model years from the result of the basic experiment.

[18] Based on the measurements in the Sea of Okhotsk [*Fujisaki et al.*, 2009], the air-ice drag coefficient $C_{Dai} \times 10^3$ of 2, 3 (basic), 4, and 5 are tested. In terms of the ice-water drag coefficient, $C_{Diw}, \times 10^3$ of 3, 6, and 9 (basic) are tested based on the empirical ratio of C_{Dai} to C_{Diw} that ranges from 0.2 to 0.8 in geostrophic reference [*Leppäranta*, 2005].

[19] We assume C_{Dai} and C_{Diw} are constants, not a function of the stratifications, because the stratifications of the boundary layers over and under ice during winter are unstable and C_{Dai} and C_{Diw} are always close to the neutral values. A summary of the numerical experiments are listed in Table 2.

3. Hindcast Through 1998–2000

3.1. Circulation and Sea Ice Extent

[20] Seasonal variation of sea ice area, ice edge position, and the volume transport of the ESC simulated in the model were already validated by *Fujisaki et al.* [2010]. Here, the validation that is important to reproduce the DSW formation will be shown.
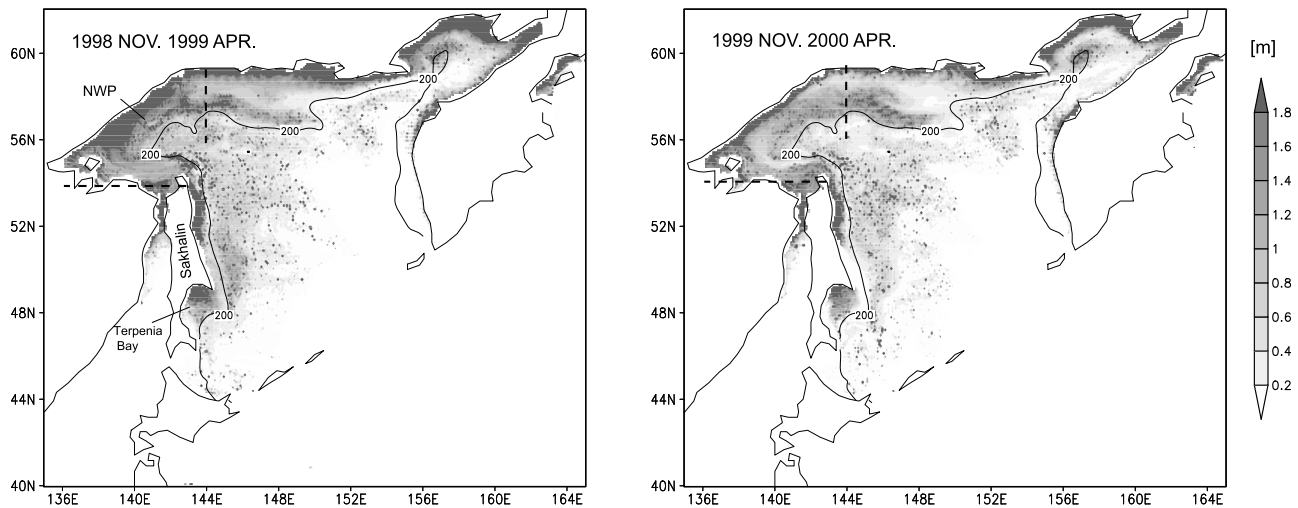
Figure 6. Annual ice productions per unit area (m). Ice production in the northwest polynya (NWP) is listed in Table 3. The NWP is defined by a surrounded shelf region and is shallower than 200 m depth.

[21] Figure 3 shows a stream function averaged from October 1998 to September 2000. The strong southward flow of the ESC is seen on the east of Sakhalin Island. On the east side, on the west of the Kamchatka, the flow is weakly northwestward. The volume transport of the ESC is significantly intensified as C_{Dai} increases [*Fujisaki et al.*, 2010]. In 1998–1999, an increase of C_{Dai} from 3×10^{-3} to 5×10^{-3} intensified the seasonal mean volume transport of the ESC almost linearly from 5.0 to 8.1 Sv [*Fujisaki et al.*, 2010, Table 3]. We will discuss in section 5 that this intensified flow could affect the density constitution of the DSW in balancing with brine rejection.

[22] The simulated ice fields agreed well with the objective sea ice analysis compiled by the Japan Meteorological Agency (Figures 4 and 5). The sea ice extent and the corresponding ice edge position is almost independent of C_{Dai} and C_{Diw} (Figure 5), and this is due to melting at the thermal front in the east side of the Sea of Okhotsk [*Fujisaki et al.*, 2010], which is likely to be influenced by warm water inflow from the North Pacific and Japan Sea.

3.2. Ice Production

[23] Figure 6 shows ice productions in the two winters from the basic experiment. Active ice formation can be seen in the northern shelf, especially in the northwest polynya region (NWP, marked in Figure 6). This is consistent with the coastal polynya activity, where the offshore motion of sea ice driven by wind promotes continuous ice formation. Such high ice production in the NWP is consistent with a climatological ice production estimated by *Ohshima et al.* [2003]. There are also significant ice productions in the east coast of the Sakhalin Island and in Terpenia Bay, which are also shown by *Ohshima et al.* [2003]. The two areas with high ice production are consistent with the polynya activities detected from the divergence of ice motion by *Kimura and Wakatsuchi* [2004]. Thus, the model reproduces the reasonable ice production. Along the northern shelf break (about 56°N, 200 m contour line), there is a region with ice production that is not as intensive as those along the coast but are significant in both winters. The similar structure is not detected in the observational estimations, possibly because the spatial resolutions are not high enough. We do not see a polynya-like open water area in the shelf break (Figure 4), while some sea ice is likely to start forming in this region (Figure 4, January). Horizontal fluctuation of wind field or preconditioning of the ocean may be able to explain these significant ice productions along the shelf break, but we will not go into detail here.

[24] Ice production in the NWP is estimated to be 2.22×10^2 km^2 from the basic experiment in 1999–2000 (Table 3).

Table 3. Annual Ice Productions Integrated From November to April[a]

	$C_{Dai} \times 10^3$				$C_{Diw} \times 10^3$			
	2.0	3.0 (Basic)	4.0	5.0	3.0	6.0	9.0 (Basic)	No Brine Rejection
	November 1998 to April 1999 (10^2 km^3)							
Total	11.1	11.8	12.3	12.6	13.4	12.7	11.8	13.9
NWP	2.73	2.90	3.01	3.19	3.23	2.96	2.90	2.88
Mean ice speed[b] (m s^{-1})	0.13	0.16	0.18	0.20	0.20	0.17	0.16	0.16
	November 1999 to April 2000 (10^2 km^3)							
Total	9.37	9.72	10.4	10.0	10.7	10.3	9.72	11.2
NWP	2.09	2.22	2.41	2.47	2.37	2.22	2.22	2.07
Mean ice speed[b] (m s^{-1})	0.10	0.12	0.14	0.15	0.16	0.13	0.12	0.12

[a]Total is the entire Sea of Okhotsk. NWP is the northwest polynya region shown in Figure 7.
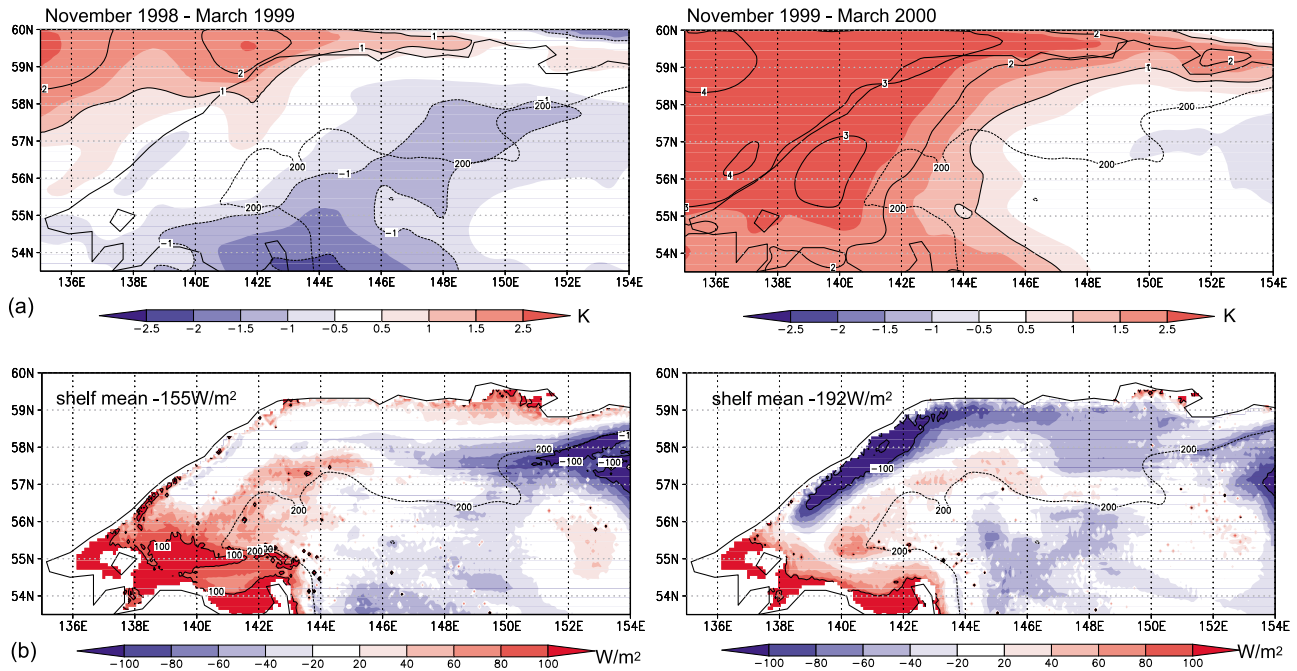[b]The mean ice speed over the NWP through December–March.

Figure 7. (a) Anomaly of winter temperature through November–March from the climatology averaged through 1996–2006, created from the objective analysis by the Regional Spectral Model compiled by the Japan Meteorological Agency. (b) Anomaly of downward heat flux at the sea surface through November–March from the mean field of 1998–1999 and 1999–2000. Mean heat fluxes over the shelf (shallower than 200 m) are shown on upper left.

This is smaller than the $3.4 \pm 0.9 \times 10^2$ km^3 estimated by *Shcherbina et al.* [2004b] based on the heat budget from satellite data. This difference may not be insignificant. *Shcherbina et al.* [2004b] might overestimate it because they did not take into account the ocean heat flux, which may not be negligible in the Sea of Okhotsk [*Fujisaki et al.*, 2010], when calculating heat balance, while the model might underestimate the ice production, and, for example, it may need to parameterize mechanical leads [e.g., *Thorndike et al.*, 1975], since it invokes strong heat loss at small scale and forms new ice more. However, we believe the differ-

ence does not hurt a generality in the process discussed for our sensitivity studies.

[25] Ice production shows a clear interannual variation that is smaller in 1999–2000 (Table 3). This is because of the milder air condition in the season, where the air temperature over the shelf regions shows a strong positive anomaly from the 10 year mean field (Figure 7a). Mean ice speed over the NWP through winter is larger in 1998–1999 (Table 3), and this may also help the larger ice production in that winter by the polynya activity. Interestingly, while the colder air in 1998–1999 formed sea ice
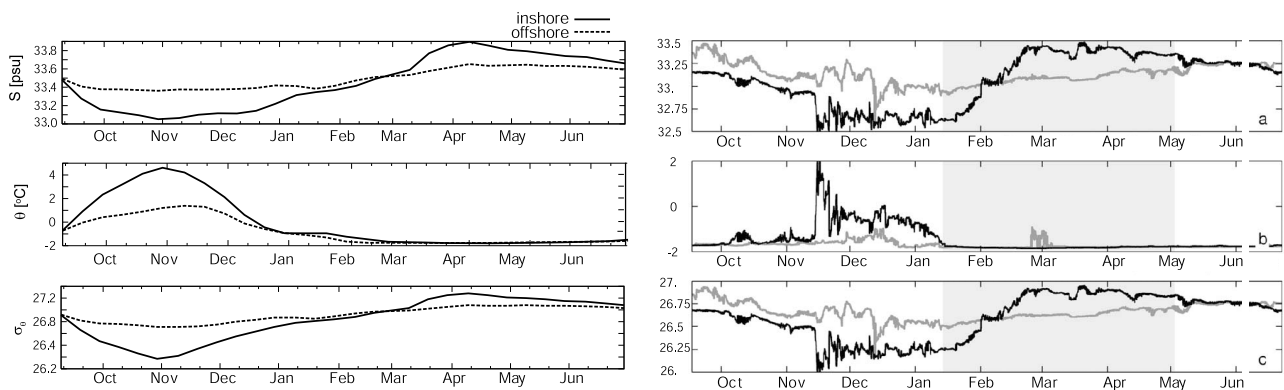

Figure 8. Salinity, potential temperature, and potential density. (left) Model results in the basic experiment from September 1999 to July 2000. (right) Observation results cited from Figure 5 of *Shcherbina et al.* [2004a] during the same period. Shading in Figure 8 (right) shows ice-covered periods. Sites are shown in Figure 10 (inshore, black star; offshore, grey star).
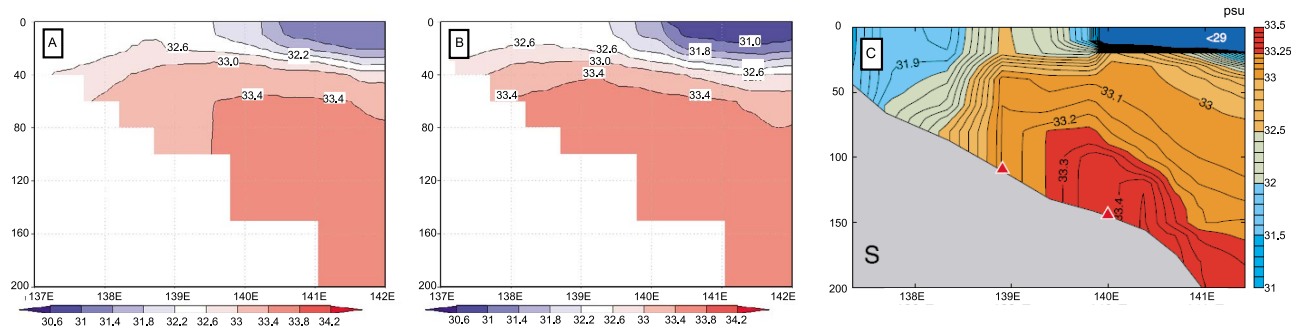
Figure 9. Vertical section of the salinity (psu) in September: the model results at 55.5°N ((a) 1999 and (b) 2000) and (c) cited from Figure 2e of *Shcherbina et al.* [2004a].

more, cooling over the shelf region is rather weak compared with that in 1999–2000 (Figure 7b). The higher ice concentration over the shelf in 1998–1999 (Figure 4, February), which is because of the larger ice production in the season, insulated heat loss from the ocean. In contrast, the lower ice concentration over the shelf in 1999–2000 allowed larger heat loss from the open water region. The variable ice productions caused negative feedback to the heat loss from the ocean by heat insulation of ice cover. This compensating heat loss for ice production may explain the interannual variability of the DSW density constitution, which is discussed in section 3.3.

3.3. Dense Shelf Water

[26] The temporal trend of the simulated bottom salinity on the shelf (Figure 8) agrees well with the observation results of *Shcherbina et al.* [2004a]. In fall, the bottom salinity drops due to the development of the mixed layer, which stirs the surface freshwater with the bottom saline water. In winter, it begins to increase due to subducted saline water. The simulated salinity is somewhat higher than the observation. As is shown in Figure 9, the model does not reproduce the thermohaline front near the coast, which is supposed to be created by the tidal mixing in summer, while it is clearly observed by *Shcherbina et al.* [2004a]. Such

coastal tidal mixing could supply the surface freshwater to the bottom during summer, and it is possible that the model overestimates the salinity field because it does not take into account the coastal tidal mixing. Nevertheless, the salinity increment from the minimum, which is dominantly influenced by DSW production, is well simulated in the model. At the same time, the model reproduces well the early fall temperature minimum at the bottom in summer (Figure 10). Salt contents over the shelf region in fall are similar in the two winters. While it is believed that preconditioning of the salinity field should determine the DSW property [*Matsuda et al.*, 2009], the resemblance of the preconditioned salinity fields in our model indicates that the DSW property here is determined mainly by air cooling and brine rejection in each winter.

[27] Figure 11 shows the time series of the DSW flux across 53°N (line A in Figure 1) on the east side of the Sakhalin Island, as well as across the lines of 143°E and 154°E (lines B and C in Figure 1) in the northern shelf. Here, DSW is defined as water colder than −1°. In terms of density, three thresholds of $26.75\sigma_\theta$, $26.85\sigma_\theta$, and $26.95\sigma_\theta$ are referenced. The DSW fluxes are significantly influenced by the seasonal variation of the ESC, which gets stronger in winter [*Mizuta et al.*, 2003]. The fluxes reach their maximum roughly in March, and decrease to zero by early
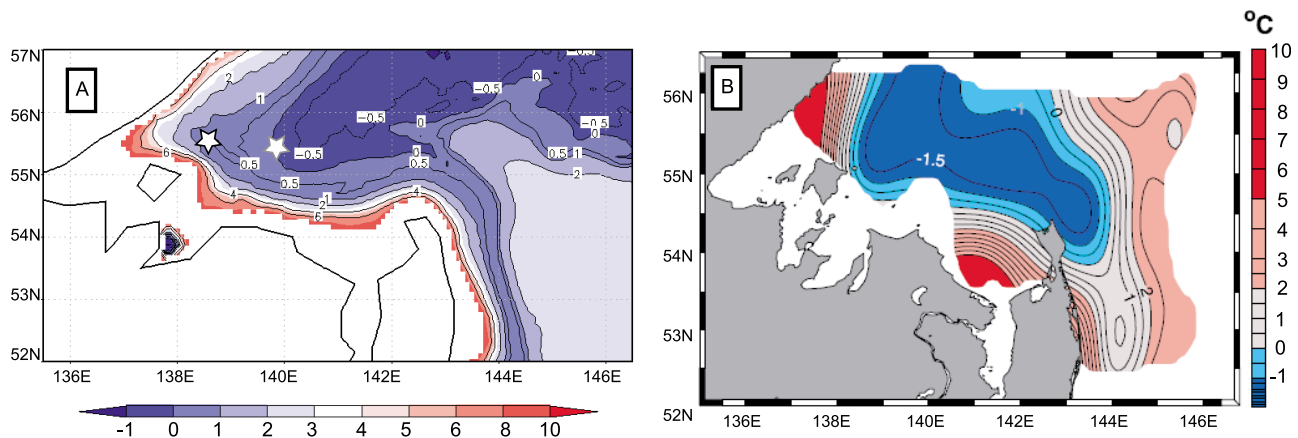

Figure 10. Potential temperature (deg) at the bottom in September 1999: (a) the model result and (b) cited from Figure 2b of *Shcherbina et al.* [2004a].
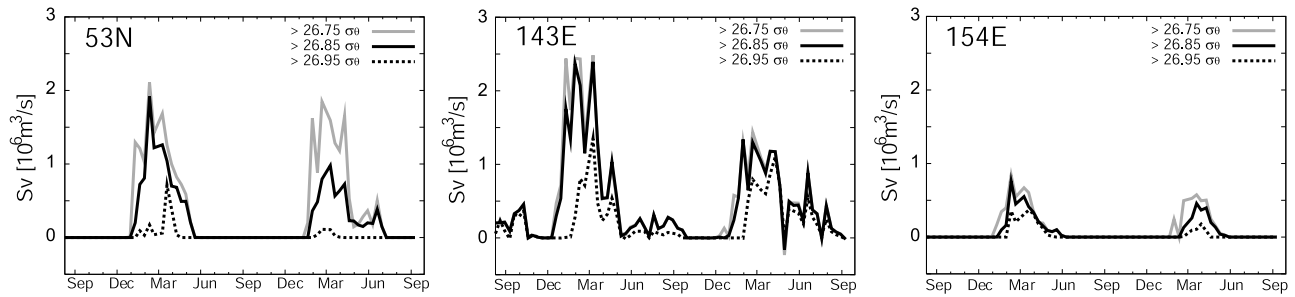
Figure 11. DSW fluxes (Sv) across the lines A (53°N), B (143°E), and C (154°E) in Figure 1 from September 1998 to September 2000.

summer. Assuming the DSW flux crosses only these three lines and the diffusion across the shelf break is negligible, we calculate the local DSW production by the following equations:

$$P_{annual} = p_{max} - p_{min} \qquad (4)$$

$$p = v(t) + \int f_{out} - f_{in} dt. \qquad (5)$$

P_{annual} is the annual production of the DSW, which is calculated by the difference between the maximum and minimum value of p, which is derived by equation (5). In most cases, p_{min} is almost zero. Here, v is the time series of the total volume of the DSW in the shelf region (northwest shelf (NWS) and northern shelf (NS) in Figure 1. Here, f_{in} and f_{out} are the time series of the inflow and outflow fluxes of the DSW across the lines A (53°N) and C (154°E). The productions calculated by equations (4) and (5) are listed in Table 4.

[28] Volumetric production of the DSW does not show a clear interannual variability (e.g., $>26.75\sigma_\theta$) in spite of clearly larger ice productions in 1998–1999, for example, by

30% for the NWP in the basic experiment. This insensitivity of DSW production is due to the heat loss that is negatively correlating against ice production (section 3.2). While ice production is smaller in 1999–2000, less developed ice cover over the shelf allows larger heat loss from the open water (Table 4 and Figure 6). Therefore, heat loss is inversely stronger in 1999–2000 due to less heat insulation. The larger heat loss from the open water in 1999–2000 fills in gaps of DSW production.

[29] However, the resulting property of the DSW is quite different because ice production thickens up the density constitution of the DSW by very dense brine, while the effect of air cooling is constrained to the lighter part. Figure 12a shows the density constitution of the DSW in the two winters. Formed DSW in 1999–2000 distributes to the relatively lighter region ($<26.8\sigma_\theta$) compared with 1998–2000, which is due to less ice production in 1999–2000. We will further discuss the effect of brine rejection based on the no brine rejection experiment (experiment 2) in section 4.

[30] Table 4 also lists DSW productions calculated without the second term in equation (5), which are marked as "no winter data." We calculated them to see the impact of

Table 4. Annual DSW Productions[a]

| | $C_{Dai} \times 10^3$ | | | | $C_{Diw} \times 10^3$ | | | |
	2.0	3.0 (Basic)	4.0	5.0	3.0	6.0	9.0 (Basic)	No Brine Rejection
	November 1998 to October 1999 (Sv)							
$>26.75\sigma_\theta$ (total)	1.23	1.33	1.24	1.28	1.31	1.33	1.33	1.17
$>26.75\sigma_\theta$ (no winter data)	1.02	1.03	1.02	1.02	1.03	1.03	1.03	0.93
$>26.85\sigma_\theta$ (total)	1.11	1.25	1.06	1.13	1.19	1.23	1.25	0.62
$>26.85\sigma_\theta$ (no winter data)	0.94	0.98	0.93	0.93	0.95	0.97	0.98	0.41
$>26.95\sigma_\theta$ (total)	0.54	0.61	0.49	0.57	0.66	0.61	0.61	0.00
$>26.95\sigma_\theta$ (no winter data)	0.54	0.61	0.49	0.57	0.66	0.61	0.61	0.00
Heat flux at sea surface over shelf (W m^{-2})	−152	−155	−162	−163	−151	−147	−155	−141
	November 1999 to October 2000 (Sv)							
$>26.75\sigma_\theta$ (total)	1.24	1.23	1.25	1.26	1.27	1.25	1.23	0.92
$>26.75\sigma_\theta$ (no winter data)	0.98	0.98	0.99	0.97	1.01	1.00	0.98	0.75
$>26.85\sigma_\theta$ (total)	1.01	0.97	1.04	0.96	1.05	1.01	0.97	0.41
$>26.85\sigma_\theta$ (no winter data)	0.84	0.82	0.83	0.76	0.90	0.85	0.82	0.28
$>26.95\sigma_\theta$ (total)	0.63	0.59	0.68	0.49	0.70	0.63	0.59	0.03
$>26.95\sigma_\theta$ (no winter data)	0.56	0.52	0.65	0.48	0.64	0.57	0.52	0.02
Heat flux at sea surface over shelf (W m^{-2})	−190	−195	−185	−198	−193	−196	−195	−200

[a]DSW is defined as colder than −1° and denser than $26.75\sigma_\theta$, $26.85\sigma_\theta$, and $26.95\sigma_\theta$. Total is the production derived by equations (4) and (5). No winter data is where the outflow of DSW (Figure 11) is neglected. Mean heat fluxes at sea surface over the shelf (135°E–154°E, shallower than 200 m depth) from December to March are also shown in Figure 7.
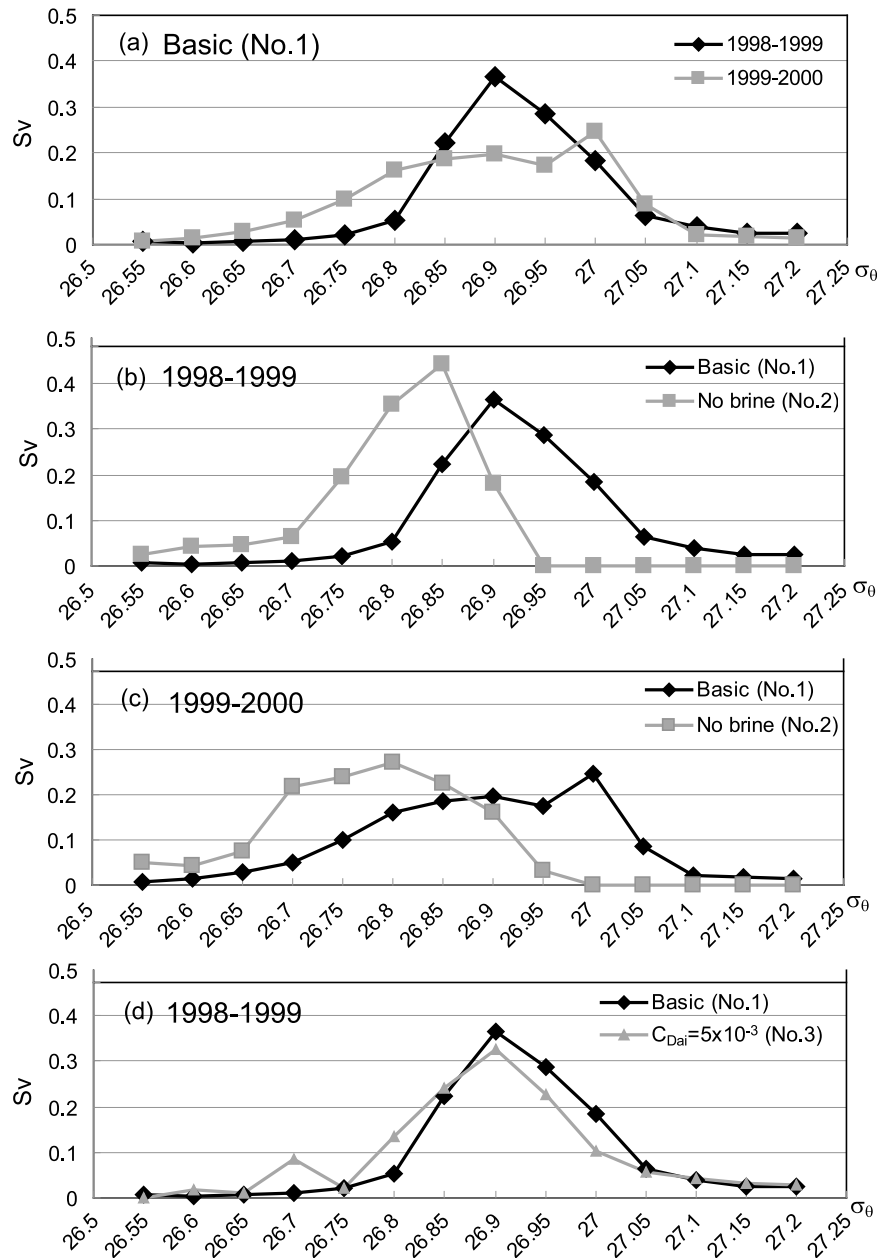
Figure 12. Annual DSW production (November–October) (Sv) at every $0.1\sigma_\theta$ potential density. (a) Interannual comparison for experiment 1 (basic experiment). Comparison of the basic experiment (experiment 1) with the no brine rejection experiment (experiment 2) in (b) 1998–1999 and (c) 1999–2000. (d) Comparison of $C_{Dai} = 3 \times 10^{-3}$ (experiment 1) and $C_{Dai} = 5 \times 10^{-3}$ (experiment 3).

excluding the winter data. It is difficult to observe the DSW fluxes during winter in reality and observational estimation of DSW production sometimes cannot utilize the information due to little in situ data [e.g., *Itoh et al.*, 2003]. For $>26.75\sigma_\theta$ and $>26.85\sigma_\theta$, DSW productions of "no winter data" are significantly underestimated (for $>26.75\sigma_\theta$, 23% in 1999 and 20% in 2000). For $>26.95\sigma_\theta$, the difference is quite small and this is due to the relatively weak DSW flux with this density threshold (Figure 11). The estimation of DSW production by *Itoh et al.* [2003] is 0.67 Sv ($>26.8\sigma_\theta$, colder than 0°), whose estimation did not take into account

the winter outflow. Such estimation might be by 20% less than actual production.

4. Sensitivity Studies

4.1. Effect of Brine Rejection

[31] The neglect of brine rejection does not change the ice production significantly (Table 3), but it significantly modifies the DSW property, contributing to the denser part of the DSW (Figures 12b and 12c). Without brine rejection (experiment 2), the denser than $26.9\sigma_\theta$ component almost disappears and most of the DSW distributes to the lighter
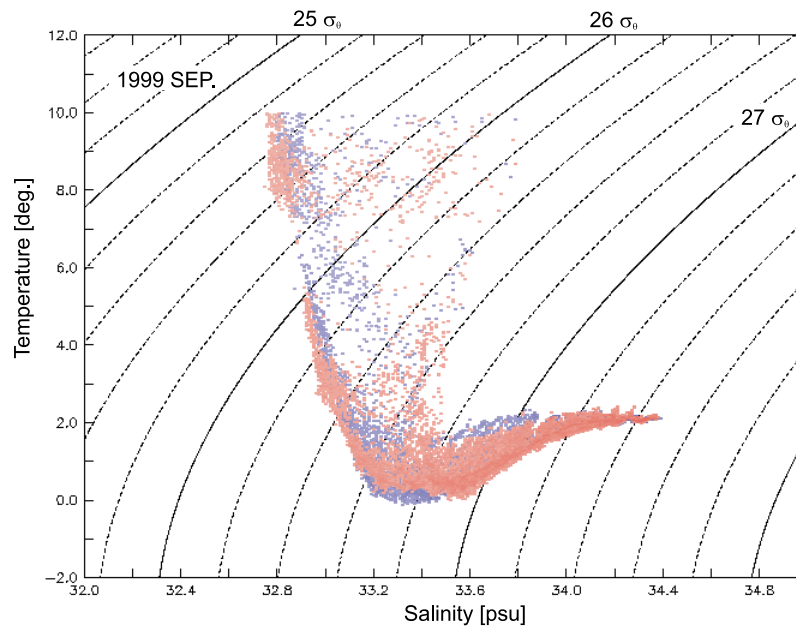
Figure 13. TS diagram in the Kuril Basin. Red is the basic experiment (experiment 1). Blue is the no brine rejection experiment (experiment 2).

part. Experiment 2 indicates that brine rejection modifies the density constitution of the DSW that is preconditioned by air cooling. Such modification by brine rejection is important for circulation of gases and nutrient materials because it determines how deep the tracers can penetrate due to brine rejection.

[32] Figure 13 shows the TS diagram in the Kuril Basin in September 1999. Most of the water mass is slightly colder when taking into account the brine rejection, except around $26.6–26.8\sigma_\theta$. The cold anomaly reached the $27\sigma_\theta$ layer. This signal by brine rejection could eventually reach the intermediate layer of the North Pacific, ventilating North Pacific Intermediate Water.

[33] Interannual variation of ice production may explain the different modification of the DSW by brine rejection. In 1998–1999, when ice production is larger, the lower than $26.8\sigma_\theta$ density DSW is almost totally transferred into the denser part by taking into account the brine rejection while it still remains in 1999–2000.

[34] DSW production decreases without brine rejection, for example, by 25% for $>26.75\sigma_\theta$ in 1999–2000 (Table 4). However, the modification of the density constitution is likely to be more important than the increase of volumetric DSW production since it determines how deep the DSW can ventilate the intermediate layer in the Kuril Basin.

[35] We should note that sea ice salinity in this study is set to zero (Table 1), while sea ice salinity measured in the Sea of Okhotsk [*Nomura et al.*, 2010] is mostly around 5 practical salinity unit (psu). Because our model sets sea ice salinity to zero it may overestimate brine rejection.

4.2. Effect of Air-Ice Coefficient C_{Dai} and Ice-Water Drag Coefficient C_{Diw}

[36] C_{Dai} and C_{Diw} measurably influenced ice production (Table 3). The ice production in the NWP is increased as C_{Dai} increases and as C_{Diw} decreases (e.g., 10% increase

from the basic experiment with $C_{Dai} = 5 \times 10^{-3}$ and $C_{Diw} = 3 \times 10^{-3}$ in 1998–1999). Total ice productions show a similar trend with C_{Dai} and C_{Diw} but are less evident compared with the NWP and there is even a reversal in 1999–2000 for $C_{Dai} = 5 \times 10^{-3}$.

[37] The increases of ice production are consistent with the expected roles of C_{Dai} and C_{Diw} on the polynya activity. Mean ice velocity over the NWP in Table 3 increases with the increase of C_{Dai} (stronger wind stress) and with the decrease of C_{Diw} (weaker water drag). This increase of velocity intensifies the offshore motion of sea ice, which is balanced by a continuous ice production to immediately fill up the open water area (Figure 14). Note that the mean ice speeds in Figure 14 are averages in January and are not identical to the seasonal averages in Table 3.

[38] On the other hand, the variation of DSW production with changing C_{Dai} and C_{Diw} is quite weak in spite of the significant trend of ice production. This is likely because of the insensitive heat loss to C_{Dai} and C_{Diw} (Table 4).

[39] Increase of ice production by C_{Dai} is expected to thicken up the DSW, but the model shows a different result. Figure 12d shows the comparison of the density constitutions of the basic experiment ($C_{Dai} = 3 \times 10^{-3}$) and the experiment of $C_{Dai} = 3 \times 10^{-3}$ (experiment 3). Increase of C_{Dai} to 5×10^{-3} shifts the density constitution to the left; i.e., increasing C_{Dai} makes the DSW lighter although it increases ice production at the same time.

[40] This is a result of a linear balance between the alongshore flow and accumulated brine in the polynya [*Kawaguchi and Mitsudera*, 2009]. The alongshore flow is likely to increase linearly with C_{Dai} as is represented in the volume transport of the ESC that intensifies by 60% with $C_{Dai} = 5 \times 10^{-3}$ from $C_{Dai} = 3 \times 10^{-3}$ (see section 3), while ice production increases only by 10%. Therefore, the dominant alongshore flow advects the dense water much faster than feeding speed of brine and, therefore, the salinity
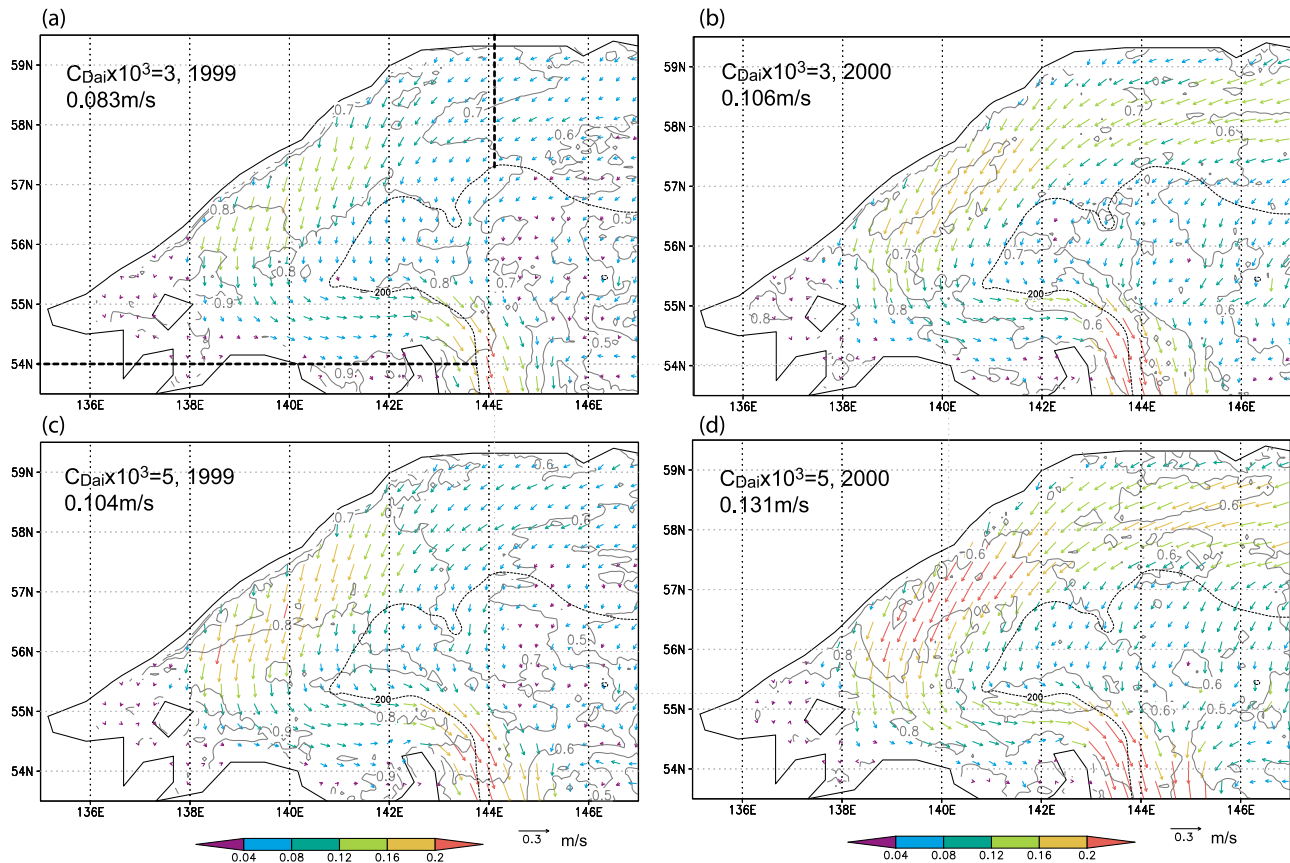
Figure 14. Mean ice velocity fields (colored vectors) in January 1999 and 2000: (a and b) $C_{Dai} = 3 \times 10^{-3}$ (experiment 1) and (c and d) $C_{Dai} = 5 \times 10^{-3}$ (experiment 3). Ice concentration is shown by a thin contour with interval of 0.1, and the contour of 200 m depth is shown by dashed line. Mean ice velocity over the NWP, which is surrounded by a thick dashed line in Figure 14a (135°E–144°E, 54°N–60°N, shallower than 200 m), is shown on upper left.

anomaly beneath the polynya is reduced. Since the density is mainly determined by salinity near freezing temperature, this reduced salinity anomaly shifts the density constitution of the DSW to the lighter part.

[41] In spite of the broad range where C_{Dai} and C_{Dai} are changed, the variations of ice production and the DSW property are relatively small. Rather, it seems the anomalous air conditions in the two seasons control the ice production, volumetric production, and density constitution of the DSW. The air temperature fields in winter controlled ice productions, as well as the mean ice speeds over the NWP, which is likely to be controlled by wind speed and direction over the polynya. The insensitivity of the DSW property to C_{Dai} and C_{Dai} reduces the uncertainty in modeling the DSW formation. However, it should be noted that the circulation increases almost linearly with C_{Dai} as is represented by the intensification of the ESC. Such significant variation may change the DSW transportation to the southern part of the Sea of Okhotsk and the ventilation of the North Pacific Intermediate Water.

5. Conclusions

[42] The DSW formation process in the Sea of Okhotsk was studied with a high-resolution ice-ocean coupled model. The model reasonably reproduced sea ice extent and the active ice production on the shelf regions. The modeled seasonal variation of bottom salinity on the shelf was consistent with the observation by *Shcherbina et al.* [2004a]. When the DSW fluxes across the shelf region in winter were excluded, as is often the case for observational estimations, the annual DSW production was underestimated by roughly 20%.

[43] The hindcast through 1998–2000 showed that ice production over the NWP was controlled by the anomalous air temperature fields and the mean ice speeds over the polynya. Ice production was less in 1999–2000 due to the warmer air temperature and the smaller ice speed over the NWP in that season, and the density constitution of the DSW in 1999–2000 distributed to the lighter part compared with that in 1998–1999.

[44] However, the volumetric DSW productions for $>26.75\sigma_\theta$ were quite similar in the two seasons. This is because heat insulation by ice cover was less in 1999–2000 due to the low ice concentration, and, therefore, the larger heat loss in 1999–2000 filled in gaps of DSW production, instead of lessening ice production, and so sustained similar production to that in 1999–2000 for the DSW for $>26.75\sigma_\theta$. Thus, ice production and heat loss from the ocean are likely

to compensate each other in terms of the volumetric production of the DSW.

[45] On the other hand, the density constitution of the DSW was controlled by ice production. The larger ice production in 1998–1999 thickened up the DSW and the density constitution distributed mostly at $>26.8\sigma_\theta$, while it significantly remained at $<26.8\sigma_\theta$ in 1999–2000. The no brine rejection experiment showed that the interannual variation of ice production was reflected in the different extent of modification of the density constitution, where larger ice production in 1998–1999 showed a clearer shift to the denser part ($>26.85\sigma_\theta$), but smaller ice production in 1999–2000 left significant production within the lighter part ($<26.85\sigma_\theta$). The effect of density modification reached farther south in the Kuril Basin, where the $27\sigma_\theta$ layer was cooled with brine rejection, suggesting that brine rejection contributes to the deep penetration of atmospheric gases and nutrient materials.

[46] Ice production in the NWP slightly increased by stronger wind stress (the larger air-ice drag coefficient C_{Dai}) and weaker oceanic stress (the smaller ice-water drag coefficient C_{Diw}) on sea ice. This is consistent with the expected polynya activity. On the other hand, the sensitivities of DSW production to C_{Dai} and C_{Diw} were weak due to the insensitive heat loss over the NWP to C_{Dai} and C_{Diw}.

[47] Stronger wind stress with $C_{Dai} = 5 \times 10^{-3}$ slightly lightened the DSW as a balance of the intensified alongshore flow, which is represented by a 60% increase of the ESC volume transport in 1998–1999, and feeding speed of brine, which is represented by a 10% increase of ice production in the same period. However, it seemed that the DSW property was insensitive to the drag coefficients, compared to the anomalous air conditions year by year.

References

Fujisaki, A., H. Yamaguchi, T. Toyota, A. Futatsudera, and M. Miyanaga (2009), Measurements of air-ice drag coefficient over the ice-covered Sea of Okhotsk, *J. Oceanogr.*, *65*, 487–498, doi:10.1007/s10872-009-0042-8.

Fujisaki, A., H. Yamaguchi, and H. Mitsudera (2010), Numerical experiment of air-ice drag coefficient and its impact on ice-ocean coupled system in the Sea of Okhotsk, *Ocean Dyn.*, *60*, 377–394, doi:10.1007/s10236-010-0265-7.

Fukamachi, Y., G. Mizuta, K. I. Ohshima, L. D. Talley, S. C. Riser, and M. Wakatsuchi (2004), Transport and modification processes of dense shelf water revealed by long-term moorings off Sakhalin in the Sea of Okhotsk, *J. Geophys. Res.*, *109*, C09S10, doi:10.1029/2003JC001906.

Gladyshev, S., S. Martin, S. Riser, and A. Figurkin (2000), Dense water production based on the northern Okhotsk shelves: Comparison of ship-based spring-summer observations for 1996 and 1997 with satellite observations, *J. Geophys. Res.*, *105*(C11), 26,281–26,299, doi:10.1029/1999JC000067.

Gladyshev, S., L. Talley, G. Kantakov, G. Khen, and M. Wakatsuchi (2003), Distribution, formation, and seasonal variability of Okhotsk Sea Mode Water, *J. Geophys. Res.*, *108*(C6), 3186, doi:10.1029/2001JC000877.

Hunke, E. C., and J. K. Duckowicz (1997), An elastic-viscous-plastic model for sea ice dynamics, *J. Phys. Oceanogr.*, *27*, 1849–1867, doi:10.1175/1520-0485(1997)027<1849:AEVPMF>2.0.CO;2.

Itoh, M., K. I. Ohshima, and M. Wakatsuchi (2003), Distribution and formation of Okhotsk Sea Intermediate Water: An analysis of isopycnal climatological data, *J. Geophys. Res.*, *108*(C8), 3258, doi:10.1029/2002JC001590.

Kawaguchi, Y., and H. Mitsudera (2009), Effects of along-shore wind on DSW formation beneath coastal polynyas: Application to the Sea of Okhotsk, *J. Geophys. Res.*, *114*, C10013, doi:10.1029/2008JC005041.

Kimura, N., and M. Wakatsuchi (2004), Increase and decrease of sea ice area in the Sea of Okhotsk: Ice production in coastal polynyas and dynamic thickening in convergence zones, *J. Geophys. Res.*, *109*, C09S03, doi:10.1029/2003JC001901.

Large, W. G., and S. Pond (1981), Open ocean momentum flux measurements in moderate to strong winds, *J. Phys. Oceanogr.*, *11*, 324–336, doi:10.1175/1520-0485(1981)011<0324:OOMFMI>2.0.CO;2.

Leppäranta, M. (2005), *The Drift of Sea Ice*, Springer, Berlin.

Levitus, S., R. Burgett, and T. P. Boyer (1994), *World Ocean Atlas 1994*, vol. 3, *Salinity, NOAA Atlas NESDIS*, vol. 3, 111 pp., NOAA, Silver Spring, Md.

Matsuda, J., H. Mitsudera, T. Nakamura, K. Uchimoto, T. Nakanowatari, and N. Ebuchi (2009), Wind and buoyancy driven intermediate-layer overturning in the Sea of Okhotsk, *Deep Sea Res. Part I*, *56*, 1401–1418, doi:10.1016/j.dsr.2009.04.014.

Mizuta, G., Y. Fukamachi, and K. I. Ohshima (2003), Structure and seasonal variability of the East Sakhalin Current, *J. Phys. Oceanogr.*, *33*, 2430–2445, doi:10.1175/1520-0485(2003)033<2430:SASVOT>2.0.CO;2.

Nakamura, T., and T. Awaji (2004), Tidally induced diapycnal mixing in the Kuril Straits and its role in water transformation and transport: A three-dimensional nonhydrostatic model experiment, *J. Geophys. Res.*, *109*, C09S07, doi:10.1029/2003JC001850.

Nakamura, T., T. Toyoda, Y. Ishikawa, and T. Awaji (2006), Effects of tidal mixing at the Kuril Straits on the North Pacific ventilation: Adjustment of intermediate layer revealed from numerical experiments, *J. Geophys. Res.*, *111*, C04003, doi:10.1029/2005JC003142.

Nakanowatari, T., K. I. Ohshima, and M. Wakatsuchi (2007), Warming and oxygen decrease of intermediate water in the northwestern North Pacific, originating from the Sea of Okhotsk, 1955–2004, *Geophys. Res. Lett.*, *34*, L04602, doi:10.1029/2006GL028243.

Nishioka, J., et al. (2007), Iron supply to the western subarctic Pacific: Importance of iron export from the Sea of Okhotsk, *J. Geophys. Res.*, *112*, C10012, doi:10.1029/2006JC004055.

Nomura, D., J. Nishioka, M. A. Granskog, A. Krell, S. Matoba, T. Toyota, H. Hattori, and K. Shirasawa (2010), Nutrient distributions associated with snow and sediment layers in sea ice of the southern Sea of Okhotsk, *Mar. Chem.*, *119*, 1–8, doi:10.1016/j.marchem.2009.11.005.

Ohshima, K. I., T. Watanabe, and S. Nihashi (2003), Surface heat budget of the Sea of Okhotsk during 1987–2001 and the role of sea ice on it, *J. Meteorol. Soc. Jpn.*, *81*(4), 653–677, doi:10.2151/jmsj.81.653.

Sagawa, G. (2007), Development of ice dynamic model that takes account of floe collision and its validation in numerical sea ice forecast in the Sea of Okhotsk, Ph.D. thesis, Univ. of Tokyo, Tokyo.

Semtner, A. J. (1976), A model for the thermodynamic growth of sea ice in numerical investigations of climate, *J. Phys. Oceanogr.*, *6*, 379–389, doi:10.1175/1520-0485(1976)006<0379:AMFTTG>2.0.CO;2.

Shcherbina, A. Y., L. D. Talley, and D. L. Rudnick (2003), Direct observations of North Pacific ventilation: Brine rejection in the Okhotsk Sea, *Science*, *302*(5652), 1952–1955, doi:10.1126/science.1088692.

Shcherbina, A. Y., L. D. Talley, and D. L. Rudnick (2004a), Dense water formation on the northwestern shelf of the Okhotsk Sea: 1. Direct observations of brine rejection, *J. Geophys. Res.*, *109*, C09S08, doi:10.1029/2003JC002196.

Shcherbina, A. Y., L. D. Talley, and D. L. Rudnick (2004b), Dense water formation on the northwestern shelf of the Okhotsk Sea: 2. Quantifying the transports, *J. Geophys. Res.*, *109*, C09S09, doi:10.1029/2003JC002197.

Shirasawa, K. (1981), Studies on wind stress on sea ice, *Low Temp. Sci. Ser. A*, *40*, 101–118.

Thorndike, A. S., D. A. Rothrock, G. A. Maykut, and R. Colony (1975), The thickness distribution of sea ice, *J. Geophys. Res.*, *80*(33), 4501–4513, doi:10.1029/JC080i033p04501.

Uchimoto, K., H. Mitsudera, N. Ebuchi, and Y. Miyazawa (2007), Anticyclonic eddy caused by the Soya Warm Current in an Okhotsk OGCM, *J. Oceanogr.*, *63*, 379–391, doi:10.1007/s10872-007-0036-3.

Yamamoto-Kawai, M., S. Watanabe, S. Tsunogai, and M. Wakatsuchi (2004), Chlorofluorocarbons in the Sea of Okhotsk: Ventilation of the intermediate water, *J. Geophys. Res.*, *109*, C09S11, doi:10.1029/2003JC001919.

A. Fujisaki, Cooperative Institute for Limnology and Ecosystems Research, School of Natural Resources and Environment, University of Michigan, Great Lakes Environmental Research Laboratory, NOAA, Room 305, 4840 S State Rd., Ann Arbor, MI 48108, USA. (ayumi.fujisaki@noaa.gov)

H. Mitsudera, Institute of Low Temperature Science, Hokkaido University, Kita-19, Nishi-8, Kita-ku, Sapporo 060-0819, Japan. (humiom@lowtem.hokudai.ac.jp)

H. Yamaguchi, Graduate School of Frontier Science, the University of Tokyo, 5-1-5 Kashiwanoha, Kashiwa-shi, Chiba-ken, Tokyo 277-8561 Japan. (h-yama@k.u-tokyo.ac.jp)